

Azimuthal and temporal sound fluctuations on the Chukchi continental shelf during the Canada Basin Acoustic Propagation Experiment 2017

Mohsen Badiey, Lin Wan, Sean Pecknold, et al.

Citation: [The Journal of the Acoustical Society of America](#) **146**, EL530 (2019); doi: 10.1121/1.5141373

View online: <https://doi.org/10.1121/1.5141373>

View Table of Contents: <https://asa.scitation.org/toc/jas/146/6>

Published by the [Acoustical Society of America](#)

ARTICLES YOU MAY BE INTERESTED IN

[Machine learning in acoustics: Theory and applications](#)

The Journal of the Acoustical Society of America **146**, 3590 (2019); <https://doi.org/10.1121/1.5133944>

[A propagation matrix method for the solution of the parabolic equation in ocean acoustics](#)

The Journal of the Acoustical Society of America **146**, EL464 (2019); <https://doi.org/10.1121/1.5139190>

[Observations of phase and intensity fluctuations for low-frequency, long-range transmissions in the Philippine Sea and comparisons to path-integral theory](#)

The Journal of the Acoustical Society of America **146**, 567 (2019); <https://doi.org/10.1121/1.5118252>

[Channel distortion on target scattering amplitude in shallow water](#)

The Journal of the Acoustical Society of America **146**, EL470 (2019); <https://doi.org/10.1121/1.5139200>

[Source localization by matching sound intensity with a vertical array in the deep ocean](#)

The Journal of the Acoustical Society of America **146**, EL477 (2019); <https://doi.org/10.1121/1.5139191>

[Nonlinear time-warping made simple: A step-by-step tutorial on underwater acoustic modal separation with a single hydrophone](#)

The Journal of the Acoustical Society of America **147**, 1897 (2020); <https://doi.org/10.1121/10.0000937>



**Advance your science and career
as a member of the**

ACOUSTICAL SOCIETY OF AMERICA

LEARN MORE



Azimuthal and temporal sound fluctuations on the Chukchi continental shelf during the Canada Basin Acoustic Propagation Experiment 2017

Mohsen Badiey,^{1,a)} Lin Wan,¹ Sean Pecknold,² and Altan Turgut³

¹*Department of Electrical and Computer Engineering, University of Delaware, Newark, Delaware 19716, USA*

²*Defence Research and Development Canada, Dartmouth, Nova Scotia, Canada*

³*Naval Research Laboratory, Washington DC, 20375, USA*

badiey@udel.edu, wan@udel.edu, sean.pecknold@drdc-rddc.gc.ca, altan.turgut@nrl.navy.mil

Abstract: The Shallow Water Canada Basin Acoustic Propagation Experiment was conducted on the Chukchi Sea continental shelf from October 2016 to November 2017. The experimental goals were to access (1) long-range (basin-scale) and (2) short-range (shallow-water) spatial and temporal energy variation. This letter focuses on a 20-dB energy change of acoustic signals in the frequency band 700–1100 Hz from June to August 2017 occurring along two shallow-water tracks from a common source, correlated with the occurrence of an oceanographic event in the top 150-m water column due to a Pacific Water outflow from the Bering Sea and retreat of the Marginal Ice Zone.

© 2019 Acoustical Society of America

[DRB]

Date Received: October 25, 2019 **Date Accepted:** November 23, 2019

1. Introduction

Studying shallow water acoustic waveguides has been a topic of scientific interest for several decades.¹ In that regard, establishing relationships between oceanographic variability and acoustic wave propagation is an important question.² In acoustical oceanography, temporal and spatial variability of the sound speed profile links the physical oceanographic parameters to sound propagation. Spatial and temporal variability in the sound speed profile or changing bathymetry in the horizontal plane can cause various propagation effects.³ However, very few cases have shown the simultaneous measurements of acoustic signal propagation along with detailed oceanographic measurements in complex waveguide environments.

The Arctic environment has been going through major changes over the past several decades. A number of oceanographic observations have been conducted on and around the Beaufort Sea and Chukchi Sea continental shelves with good examples shown in Refs. 4 and 5. In those regions, the variability of the water column, sea ice, and bathymetric changes along an acoustic track creates a complex acoustic waveguide. Here, we present results from a subset of a yearlong experiment conducted on the Chukchi Sea shelf where simultaneous measurements of acoustic signal propagation and oceanographic parameters were made. A significant acoustic energy fluctuation (around 20 dB) is reported during a time period when the warm Pacific Water outflow from the Bering Sea entered the acoustic source-receiver tracks. Understanding the detailed mechanism of this energy fluctuation is a key in providing future acoustical oceanography and potential tomography on the arctic shelf break region. In addition to the large energy fluctuation, it is important to point out the azimuthal dependence of the acoustic signal on the oceanographic temporal variability. The same source signature shows strong temporal variability at different receivers separated by 30°.

In Secs. 2 and 3, we present the simultaneously measured environmental and acoustic data and analyses of the observed data. Section 4 presents a summary.

2. Environmental data

Simultaneously conducted with a separate, deep-water experiment, the Shallow Water Canada Basin Acoustic Propagation Experiment (SW CANAPE) was performed over the period of October 15, 2016 through November 11, 2017 to quantify the propagation of sound signals in variable oceanographic conditions, including the shelf region

^{a)} Author to whom correspondence should be addressed.

of the Chukchi Sea and the adjacent shelf region.⁶ The goals of the experiment were two-fold: (1) to study broadband signal propagation from a deep water to a shallow water (SW) region and (2) to assess propagation of broadband sound signals in a shallow water region of the Chukchi shelf in the presence of variable oceanography. In this paper, we focus on a 20-dB acoustic signal energy variation that occurred from June 29–August 20, 2017 along two acoustic tracks extending from the 123-m through the 224-m isobaths. These tracks were separated by 30° on the Chukchi Sea shelf, emanating from a common source. The observed energy variation is correlated with the occurrence of a large oceanographic event spanning the top 150 m of the water column due to a Pacific Water outflow from the Bering Sea and the retreat of the Marginal Ice Zone during the aforementioned observation period. During the experiment, the University of Delaware (UD) array of oceanographic moorings (UD1–UD5 and UD7) on the continental shelf measured the temporal and spatial variability of the environment. We focus our analysis on the signals emitted from one of the two SW sources provided by the U.S. Naval Research Laboratory (NRL S2 in Fig. 1) and received by two SW Autonomous Multichannel Acoustic Recorder (AMAR) arrays (R2 and R3 in Fig. 1, with an array separation of 15.8 km) to show the directionality of the acoustic wave propagation in this region. We consider two 32-km acoustic tracks (S2-R2 and S2-R3) defined by two sides of a 30° sector where the common acoustic source was placed at the apex (S2) and the maximum spatial and temporal variation of acoustic energy was observed at R2 and R3 (see Fig. 1). Water column temperature profiles were measured at various depths at the source (S2) and two oceanographic moorings (i.e., UD1 and UD3). As shown in Figs. 1 and 2, AMAR2 and AMAR3 were close to UD1 and UD3, respectively. The inset of Fig. 1 shows water depth along the two sound propagation tracks. One was along the 100-m isobath in water depth ranging from 156 to 123 m and the other crossed the 200-m isobath in water depth ranging from 156 to 224 m. Table 1 summarizes the coordinates of the experimental assets. Figure 2 shows Sentinel-1 satellite⁷ images of surface ice evolution overlaid by the positions of the acoustic sources, receivers, and sound propagation tracks for four different geotimes (i.e., June 29, July 6, July 11, and July 29). Satellite image processing, including calibration, speckle filtering, and terrain correction, has been applied to the raw image data. Figures 3(a)–3(f) show simultaneously measured waveguide parameters starting from the daily sea ice concentration Fig. 3(a) obtained from the European Organization for the Exploitation of Meteorological Satellites Ocean and Sea Ice Satellite Application Facility.⁸ These data are reported on a 10 × 10 km grid at a time scale of 1 day. Figure 3(a) shows the reduction of surface ice from above 60% in the beginning of July to a no-ice condition (0%) after July 22, 2017. This percentage of ice coverage reduction is consistent with the available Sentinel satellite images from specific days during this period (see Fig. 2). We also notice that prior to the ice melt there are strong

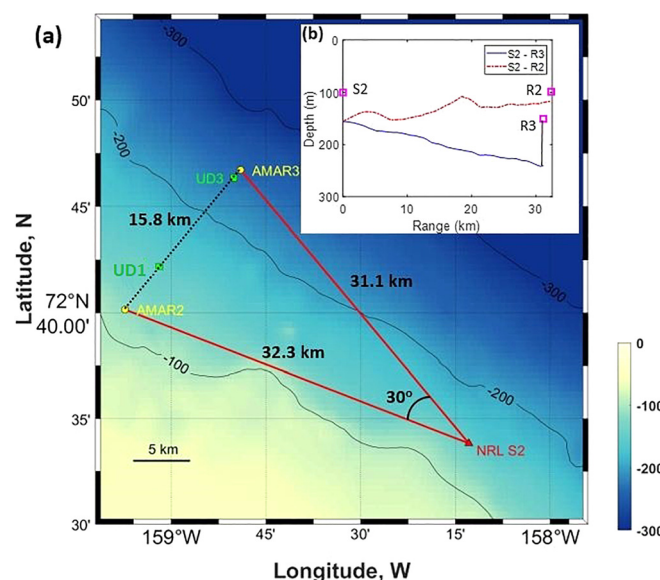


Fig. 1. (Color online) (a) Experimental configuration showing locations of the sound source (S2), the receiver arrays (R2 and R3), and the environmental sensors (UD1 and UD3). (b) Bathymetry of the two waveguides' cross sections (S2-R2 shown as a dashed-dotted curve and S2-R3 shown as a solid curve). Locations of the source and each receiver array in water column are marked as squares.

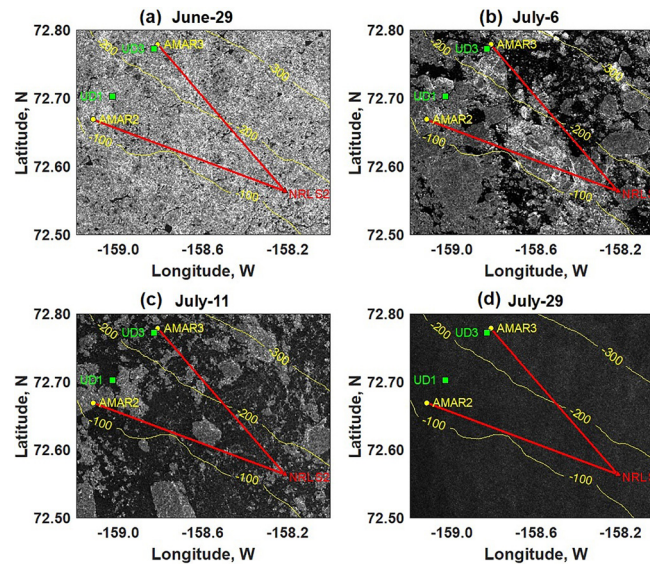


Fig. 2. (Color online) Sentinel-1 satellite images of surface ice evolution overlaid by the positions of acoustic source, receivers, and the sound propagation tracks for four different geotimes. The contour lines indicate depth isobaths (m). The reduction of surface ice was observed at different geotimes from (a) to (d).

oceanographic features in the water column depicted by the temperature profiles in Figs. 3(b), 3(c), and 3(d). These profiles were low-pass filtered using a fourth order Butterworth filter, downsampled to hourly, and plotted as a function of depth and time (from June 29, 2017 12:00 UTC to August 20, 2017 12:00 UTC) at S2, UD3, and UD1, respectively. The depths of the temperature sensors are marked as circles. The salinity in the upper and lower water column was recorded by two CTD sensors (marked as up triangles) on each environmental array.

3. Acoustic data

The acoustic source S2, deployed on the continental shelf, transmitted linear frequency modulated (LFM) signals in two frequency bands: (1) 700–1100 Hz and (2) 1.5–4 kHz. The S2 source broadcasted down sweeping LFM signals with duration of 2 s for 12 min every 4 h, every day of the year. The nominal source depth was 100 m and is marked as a square in Fig. 3(b); the hydrophone depths are marked as squares in Fig. 3(c) for R3 and in Fig. 3(d) for R2. Here, we focus on the LFM data in the frequency band of 700–1100 Hz. The acoustic signals from S2 were recorded at a sampling rate of 16 kHz. The acoustic data recorded by channel 5 of the AMARs (at a depth of 150.8 m for R3 and 98.8 m for R2) are utilized. The left panel of Figs. 3(e) and 3(f) shows the spectrogram and the energy level of the match filtered signals (the impulse response) as a function of geotime for the acoustic transmissions along S2-R3 and S2-R2, respectively. We calculate the acoustic energy of each pulse using⁹

$$E(T_g) = \int_{f_1}^{f_2} E_0(f, T_g) df, \quad (1)$$

where f_1 and f_2 are the lower (700 Hz) and upper (1100 Hz) frequency limits of the signal. $E_0(f, T_g)$ is the energy spectral density as a function of frequency at geotime T_g . The acoustic energy is obtained by integrating E_0 over the frequency band (700–1100 Hz). The black circles in the left panel of Figs. 3(e) and 3(f) represent the acoustic energy level (i.e., $10 \cdot \log[E(T_g)]$) in units of dB. Correspondingly, the curves in the right panel show the energy spectral density level [i.e., $10 \cdot \log(E_0)$] at selected geotimes (June 29, July 11,

Table 1. Locations of the experimental assets used in this paper.

Assets	Long. (°)	Lat. (°)	Sensor Depth (m)	Water Depth (m)
UD1	−159.0318	72.7029	23 to 137	145
UD3	−158.8346	72.7726	21 to 211	219
AMAR2	−159.1219	72.6693	91 to 109	123
AMAR3	−158.8166	72.7787	136 to 171	224
NRL S2	−158.2143	72.5638	72 to 147	156

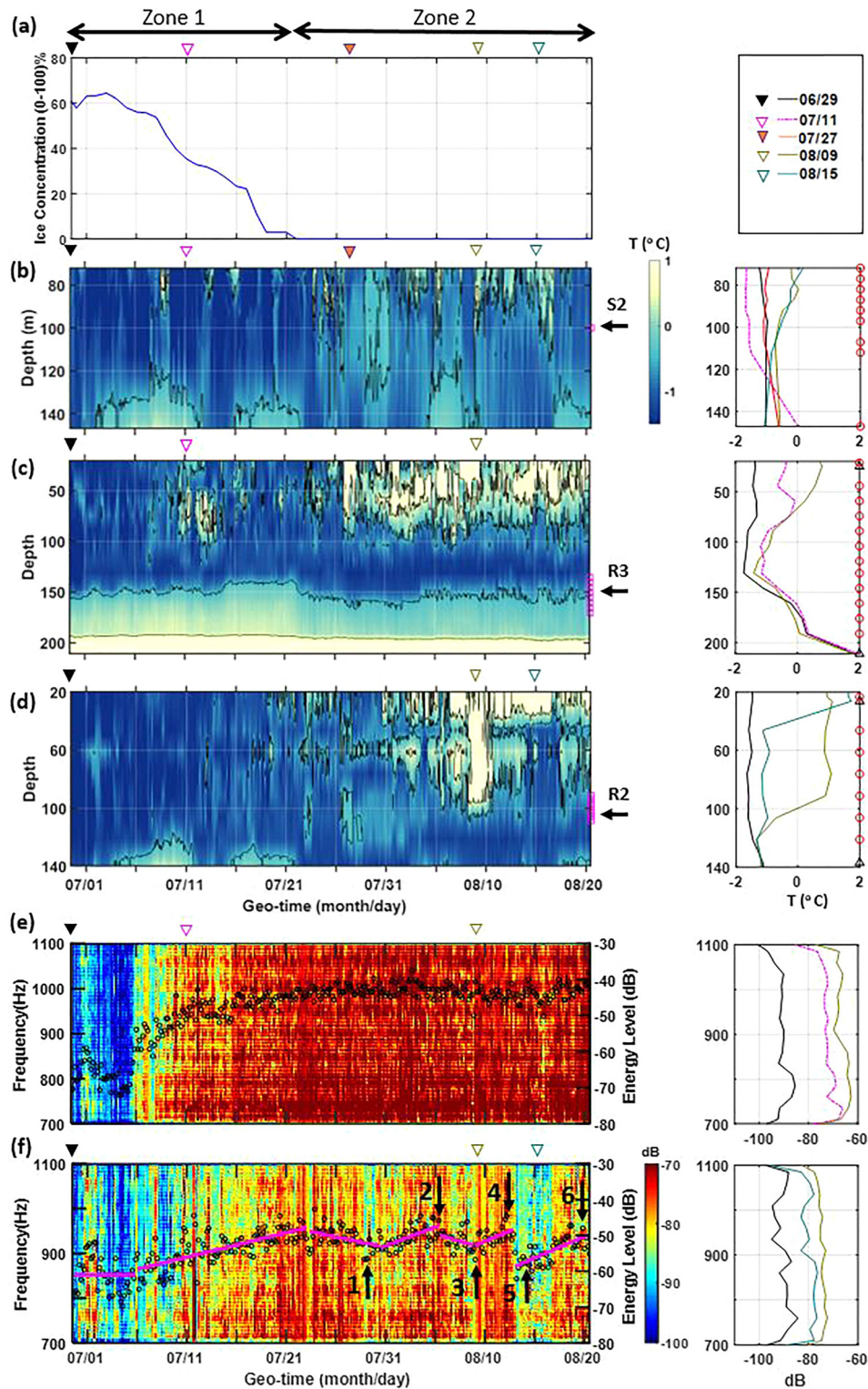


Fig. 3. (Color online) (a) The daily ice concentration obtained from atmospherically corrected Special Sensor Microwave Imager and Sounder (SSMIS) brightness temperatures. Two geotime zones (1 and 2) corresponding to sea surface (ice-covered and ice-free) conditions are defined (zone 1 from June 29 to July 22, 2017, and zone 2 from July 22 to August 20, 2017), respectively. (b), (c), and (d) Temperature as a function of depth and time at S2, UD3, and UD1, respectively. Sensors are marked as circles and up triangles. (e) and (f) Spectrogram and energy of the impulse response for the acoustic transmissions along S2-R3 and S2-R2, respectively.

August 9 for S2-R3; and June 29, August 9, August 15 for S2-R2). It is noted that the signal energy level at two receiver arrays separated by around 32 km from the same source is drastically different due to the spatial, temporal, and three-dimensional effects. These effects include the changes in bathymetry [see Fig. 1(a)] and surface roughness between source and each receiver array as well as the temperature profiles along each track.

Three geotimes (i.e., June 29, July 11, August 9) are selected to explain the fluctuation along the S2-R3 track. These geotimes corresponded to various stages of surface ice from partial coverage to the ice-free sea surface condition. A 20-dB increase in acoustic energy is observed in both the left and right panels of Fig. 3(e), mainly due to the formation of the sound duct centered at 120 m. In the right panel of Fig. 3(c), the temperature profiles at these three geotimes indicate the upper 120-m water changed from iso-thermal on June 29 to downward refracting on August 9 while the lower water column remained upward refracting. Thus, the sound propagation was focused in this new, subsurface sound duct during the ice-free condition (i.e., 0% ice concentration after July 22). The energy fluctuation along the S2-R2 track shows entirely different patterns [see Fig. 3(f)]. The magenta curves, obtained by least-square fittings to the energy data, indicate a 10 dB increase in signal energy from July 5 to July 22. During the ice-free time period (after July 22), it exhibits a larger variation (up to 12 dB) than the other track. Six geotimes are grouped as three pairs and marked as 1 through 6 in the left panel of Fig. 3(f). Each group contains one peak and one energy trough. The slope for lines 1–2, 3–4, and 5–6 are around 1.14 dB/day. The corresponding three pairs of temperature profiles at UD1 and S2 are plotted in Figs. 4(a)–4(c). The temperature measurements at S2 were only made in a small portion of the water column [see the depths of the temperature sensors in the right panel of Fig. 3(b)]. No temperature data were obtained above 70 m and from 115 to 145 m. Thus, the temperature profiles at UD1, which were the closest environmental mooring to R2, are utilized to explain these observations. The trough energy at geotime 1 is attributed to the defocusing effect caused by the concavity of the temperature profile near 120-m water [see Fig. 4(a)]. At geotime 3, a strong thermocline (around 100 m water depth) caused a downward refracting condition that increased the interaction between the signal and seafloor, which resulted in a larger signal attenuation compared

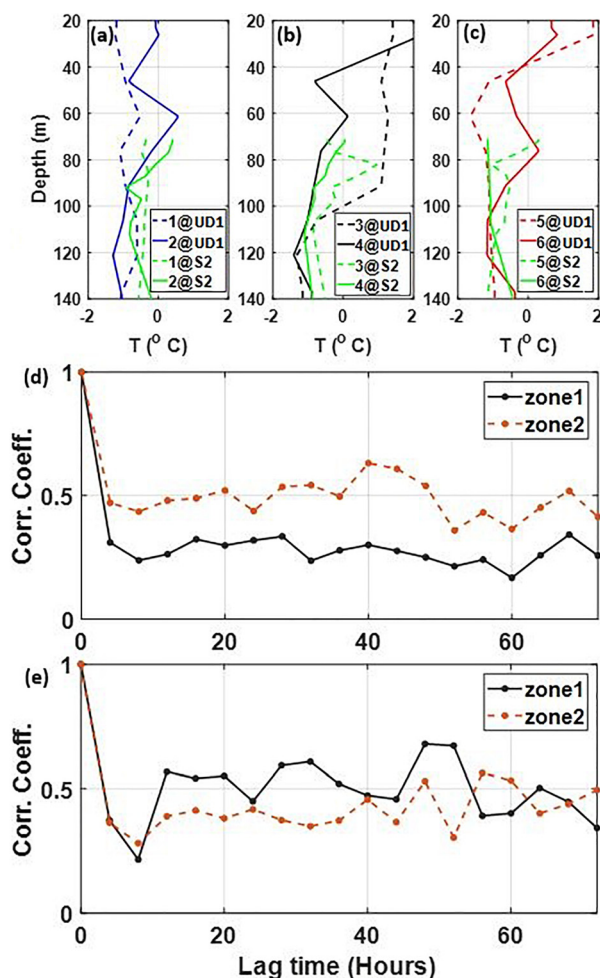


Fig. 4. (Color online) (a), (b), and (c) Temperature profiles for six different geotimes at UD1 and S2; (d) and (e) temporal correlation coefficient as a function of lag time at R3 and R2, respectively. Reference times for Zone 1 and 2 are June 29 and July 27, respectively.

to geotime 4 [see Fig. 4(b)], when the thermocline occurs around 40 m, and the signal does not suffer as much bottom interaction. The water column at geotime 5 was almost isothermal below 80 m while the temperature profile of geotime 6 reached its minimum at the depth of 120 m, close to the source depth. Therefore, more energy propagated around the temperature minimum at geotime 6 [see Fig. 4(c)].

To study the fluctuation of acoustic signals in the dynamic shallow water waveguide, we calculate the correlation coefficient as a function of lag time in the same manner as shown in Refs. 10 and 11. The correlation coefficient is obtained by the equation

$$\rho(\Delta T, \tau) = \frac{\int_0^{\Delta T} p_1(t)p_1(t + \tau)dt}{\sqrt{\int_0^{\Delta T} p_1^2(t)dt \times \int_0^{\Delta T} p_1^2(t + \tau)dt}},$$

where ΔT is the integration time, τ is the time lag, $p_1(t)$ is the reference signal received at time t , and $p_1(t + \tau)$ is the received signal with a time lag τ .

Figures 4(d) and 4(e) show the measured temporal correlation coefficient as a function of lag time at R3 and R2, respectively. We define two geotime zones [zone 1 and 2 shown in Fig. 3(a)] depicting ice-covered and ice-free conditions. The reference geotime corresponding to zero lag time for these two zones are June 29 and July 27, respectively. Figure 4(d) demonstrates higher correlation coefficient for zone 2 (ice-free) than zone 1 (60% ice coverage) along the S2-R3 track, because the effect of the fluctuations from the sea surface and bottom were mitigated due to the formation of strong sound duct in zone 2 [see Fig. 3(c)]. In zone 1, the temperature profile above 120 m shows a well-mixed layer, causing acoustic energy loss due to interaction with the surface ice. Figure 4(e) shows smaller correlation coefficients for zone 2 along the S2-R2 track, which could be due to the changes in bathymetry between source and receiver causing more bottom interaction of the acoustic signal. A different variation of the temperature profiles compared to the R2-R3 track could also contribute [see Figs. 3(c) and 3(d)].

4. Summary

This express letter presents detailed measurements of a large energy variation during SW CANAPE. The 20 dB energy change was correlated with occurrence of an oceanographic event spanning the top 150 m water column caused by a Pacific Water outflow from the Bering Sea and the retreat of the Marginal Ice Zone. Simultaneously measured acoustic propagation in the frequency band of 700–1100 Hz and oceanographic measurement of temperature in water column reveal a strong azimuthal dependence in the received signal energy from the same sound source along two separate along-shelf acoustic tracks. A clear distinction between ice-covered and ice-free conditions in the waveguide is not the only driver of the strong energy variation. Rather, the combined effects due to the oceanographic changes, as well as temporal and spatial effects, including those of the sea surface, sea bottom, and out-of-plane propagation, could be responsible. Water column oceanographic changes due to the seasonal dynamic exchange between the Pacific Water and the Atlantic Water on the Chukchi shelf along with spatial and temporal changes of sea ice and spatial variability of the sea bottom cause insonification that is azimuthally variable in geotime. It is noticed that the largest energy variability occurs during the melting of the surface ice from mid-June to mid-July, 2017. That is coincidental with the warm Pacific Water outflow and the upwelling of warm Atlantic Water around Chukchi shelf break.

Acknowledgments

This research was supported by the Office of Naval Research Ocean Acoustics Program (ONR OA322) under Grant Nos. N00014-15-1-2110, N00014-15-1-2806, N00014-15-1-2898, and N00014-18-1-2140. The authors wish to thank the crew and captains of R/V Sikuliaq and USCG Healy as well as Jim Dunn, Richard Lenhart, and Andreas Muenchow for deployment and recovery of experimental assets. We also thank the reviewers for their constructive suggestions and comments.

References and links

- ¹C. L. Pekeris, "Theory of propagation of explosive sound in shallow water," in *Propagation of Sound in the Ocean*, edited by J. L. Worzel, M. Ewing, and C. L. Pekeris (Geological Society of America, New York, 1948).
- ²W. Munk, P. Worcester, and C. Wunsch, eds., *Ocean Acoustic Tomography* (Cambridge University Press, Cambridge, England, 1995).

- ³M. Badiey, Y. Mu, J. F. Lynch, J. R. Apel, and S. Wolf, “Temporal and azimuthal dependence of sound propagation in shallow water with internal waves,” *IEEE J. Ocean. Eng.* **27**, 117–129 (2002).
- ⁴W. B. Corlett and R. S. Pickart, “The Chukchi slope current,” *Prog. Oceanogr.* **153**, 50–65 (2017).
- ⁵E. T. Brugler, R. S. Pickart, G. Moore, S. Roberts, T. J. Weingartner, and H. Statscewich, “Seasonal to interannual variability of the Pacific Water boundary current in the Beaufort Sea,” *Prog. Oceanogr.* **127**, 1–20 (2014).
- ⁶M. Badiey, A. Muenchow, L. Wan, M. S. Ballard, D. P. Knobles, and J. D. Sagers, “Modeling three dimensional environment and broadband acoustic propagation in arctic shelf-basin region,” *J. Acoust. Soc. Am.* **136**, 2317–2317 (2014).
- ⁷Information on the Sentinel-1 satellite is available at <https://sentinel.esa.int/web/sentinel/missions/sentinel-1> (Last viewed July 19, 2019).
- ⁸Information is available at <http://www.osi-saf.org/> (Last viewed July 19, 2019).
- ⁹A. V. Oppenheim and G. C. Verghese, eds., *Signals, Systems, and Inference* (Pearson Education Limited, Harlow, United Kingdom, 2017), pp. 44–46.
- ¹⁰L. Wan, J. X. Zhou, P. H. Rogers, and D. P. Knobles, “Spatial coherence measurements from two l-shape arrays in shallow water,” *Acoust. Phys.* **55**, 383–392 (2009).
- ¹¹M. Badiey, Y. Mu, J. A. Simmen, and S. E. Forsythe, “Signal variability in shallow-water sound channels,” *IEEE J. Ocean. Eng.* **25**, 492–500 (2000).